ELSEVIER

Journal of Nuclear Materials 318 (2003) 274–282

journal of nuclear materials

www.elsevier.com/locate/jnucmat

Tensile properties of ferritic/martensitic steels irradiated in HFIR, and comparison with spallation irradiation data

K. Farrell *, T.S. Byun

Oak Ridge National Laboratory, Bldg. 4500S, MS 6151, P.O. Box 2008, Oak Ridge, TN 37831, USA

Abstract

Tensile properties of four ferritic/martensitic steels, 9Cr–1MoVNb, 9Cr–1MoVNb–2Ni, 9Cr–2WV, and 9Cr–2WVTa, and two bainitic steels, 3Cr–3WV and A533B, were measured after irradiation to doses up to 1.2 dpa at temperatures in the range 60–100 °C in the High Flux Isotope Reactor and compared with two ferritic/martensitic (F/M) steels irradiated with 800 MeV protons and spallation neutrons in the LANSCE facility at 60–164 °C. Irradiation hardening in the steels was strong, and all of them displayed plastic instability shortly after yield for irradiations of 0.054 dpa and higher. Despite large loses in elongation, all failures occurred in a ductile manner. The dose dependencies of the increases in the yield strength with dpa were similar for all six steels, and contained a pronounced change at about 0.05 dpa. Below 0.05 dpa, the hardening exponent was 0.5–0.6, consistent with a barrier hardening mechanism. Above 0.05 dpa, the exponent was reduced to 0.1–0.2, which is speculated to be due to intervention by dislocation channeling. A trend curve for correlating changes in yield strengths of F/M steels with dose at irradiation temperatures below 160 °C is offered.
© 2003 Elsevier Science B.V. All rights reserved.

1. Introduction

The target vessel and proton beam window for the liquid mercury target of the proposed Spallation Neutron Source at ORNL will operate at temperatures of 100–150 °C. Substantial quantities of helium and hydrogen will be generated in the materials. The selected material for the vessel and window is 316LN austenitic stainless steel. However, in the mid-1990s when work on materials irradiations was commissioned, support for a ferritic/martensitic (F/M) target vessel was quite strong at other laboratories, so F/M materials were included in the ORNL studies.

High chromium F/M steels are based on the composition Fe–(9–12)Cr with minor alloying elements such as Mo, V, and Nb. These steels are quenched or air cooled from the austenite phase region to form martensite, which is subsequently tempered to a lath-like structure of ferrite and fine carbide precipitates. F/M steels are strong and have good resistance to aqueous corrosion. They are used in boilers and steam turbines. A very recent ASTM monograph [1] describes the use of F/M steels for nuclear power applications, and contains the most comprehensive treatment of radiation effects in the steels. F/M steels have been proposed as vessel materials for liquid–metal targets in spallation neutron sources. Their attributes for such use, compared with stainless steel, are higher strength, better thermal conductivity, lower coefficient of thermal expansion, allegedly better compatibility with liquid mercury and Pb–Bi eutectic, less radiation-induced swelling, and less residual radioactivity. Newer versions of the steels are being developed in which the minor alloying elements Mo and Nb are replaced with reduced-radioactivation elements W, Ta, and Ti. Regular ferritic steels are known to have better resistance to the deleterious effects of radiation-induced helium embrittlement at elevated temperatures, and it is assumed that this asset will prevail in F/M steels, too. The major shortcoming of F/M steels for low

* Corresponding author. Tel.: +1-865 574 5059; fax: +1-865 574 0641.

E-mail address: farrellk@ornl.gov (K. Farrell).

0022-3115/03/$ - see front matter © 2003 Elsevier Science B.V. All rights reserved.
doi:10.1016/S0022-3115(03)00102-8

temperature reactor applications is that they undergo a ductile-to-brittle transition (DBTT). Although the DBTT can be quite low for unirradiated F/M materials, say less than −50 °C, radiation-induced upshifts of more than 200 °C have been reported [1]. Such increases are caused by radiation hardening and/or radiation induced migration of impurities to grain boundaries. Radiation-produced helium is one such impurity and its effects on the DBTT are an ongoing controversy in F/M steels. Most radiation effects in F/M steels have been measured for irradiation temperatures in the range 200–450 °C. At higher temperatures, there is no radiation hardening. Transmutation products are generated at all irradiation temperatures, and their effects may be exacerbated by radiation hardening. For irradiations of F/M alloys made below 150 °C, there are almost no data for doses below 1 dpa; tensile tests after doses of 4–24 dpa displayed considerable hardening and ductility loss [2–7], and Charpy impact tests after 3–9 dpa showed increases in DBTTs of up to 140 °C [8].

The goal of the present ORNL experiments was to expand the database of F/M materials in the low irradiation temperature and lower dose regimes. Tensile results from these irradiations are reported herein.

2. Experiment details

The experiments consist of tensile tests conducted at room temperature on F/M steels irradiated with fission neutrons at temperatures of 60–100 °C. The materials were four F/M steels, 9Cr–1MoVNb, 9Cr–1MoVNb–2Ni, 9Cr–2WV, and 9Cr–2WVTa; a 3Cr–3WV bainitic steel; and a pressure vessel steel, A533B. Chemical compositions and heat treatments of the steels are listed in Table 1. All F/M materials had lath-like, tempered martensite structures. The 3Cr–3WV and A533B steels had lath structures of tempered bainite. The 9Cr–1MoVNb alloy represents the common modified 9Cr–1Mo steel (T91). The 9Cr–1MoVNb–2Ni is the 9Cr–1MoVNb steel with 2%Ni added as a dopant to promote the generation of helium from the $Ni^{58} + n_{th} \rightarrow Ni^{59}$; $Ni^{59} + n_{th} \rightarrow Fe^{56} + He^{4}$ sequential reactions in a mixed spectrum reactor. This Ni-enriched steel is involved in a dispute over the effects of helium in F/M steels, as cited in Section 3.3. The 9Cr–2WV and 9Cr–2WVTa steels are variants of low-activation F/M steels. The 3Cr–3WV steel is an experimental, low chromium, low-activation steel developed at ORNL for fusion reactor applications [9]. The A533B steel has been used extensively as a reference material in studies of radiation effects in pressure vessels. It is included here for comparative purposes.

Table 1
Chemical compositions and heat treatments of the steels

Element	(a) 9Cr–1MoVNb (Ht XA3590)	(b) 9Cr–1MoVNb–2Ni (Ht XA3591-9)	(c) 9Cr–2WV (Ht 3790)	(d) 9Cr–2WVTa (Ht 3791)	(e) 3Cr–3WV (Ht 3786G)	A533B
C	0.09	0.064	0.12	0.11	0.091	0.22
Mn	0.36	0.36	0.51	0.44	0.30	1.48
Si	0.08	0.08	0.23	0.21	0.09	0.25
S	0.004	0.004	0.007	0.008	0.009	
P	0.008	0.008	0.014	0.015	0.015	
Ni	0.11	2.17	<.01	<.01	0.02	0.68
Cr	8.62	8.57	8.95	8.90	3.05	
Mo	0.98	0.98	0.01	0.01	<.01	0.52
V	0.209	0.222	0.24	0.23	0.24	
Nb	0.063	0.066	<.01	<.01	<.01	
Ti	0.002	0.002	<.01	<.01	<.01	
Co	0.013	0.015	0.012	0.012	0.007	
Cu	0.03	0.04	0.03	0.03	0.02	
Al	0.013	0.015	0.018	0.017	0.003	
W	0.01	0.01	2.01	2.01	3.01	
Ta	–	–	–	0.06	<.01	

Steels (a) through (e) were obtained from R.L. Klueh, ORNL. The A533B steel was donated by R.K. Nanstad, ORNL from plate 02 of the 4th Heavy Section Steel Technology Program. Tensile specimens of materials (a)–(e) were heated for 1 h at 1040 °C in flowing argon and cooled to room temperature by pulling them into the cold zone. They were then reheated for 1 h at 760 °C and pulled into the cold zone and allowed to cool to room temperature. Tensile specimens of material (b) were heated for 1 h at 1040 °C in flowing argon then pulled into the cold zone until it cooled to room temperature. It was then reheated for 5 h at 700 °C and pulled into the cold zone and allowed to cool to room temperature. Tensile specimens of the A533B steel were cut from a block that had been heated for 4 h at 857–885 °C and air cooled; reheated for 4 h at 649–677 °C and air cooled; reheated for 20 h at 607–635 °C and furnace cooled to 315 °C then air cooled to room temperature.

The tensile specimens were of the flat SS-3 type with nominal gage section dimensions of 0.76 mm thick, 1.52 mm wide, and 7.62 mm long, as shown in Fig. 1. Irradiations of these specimens were conducted in the hydraulic tube facility of the High Flux Isotope Reactor (HFIR). The facility is located in the flux trap of the reactor and because the irradiation vehicles (known as rabbits) are shuttled in and out of the tube on demand, they cannot be instrumented. The fluxes of neutrons and gamma rays are exceptionally high. Gamma heating is very strong and to keep the rabbits and their contents cool they are immersed in rapidly flowing water under a high inlet pressure of 3.33 MPa. The water inlet and outlet temperatures are 49 and 69 °C. For maximum cooling, the rabbits are heavily perforated to allow the water to be in direct contact with the specimens. In such cases the temperature of the specimens is estimated to remain in the range 60–100 °C. Rusting of ferritic steels is accelerated in a radiation field. For the present experiments, it was found that despite the normally good corrosion resistance for F/M steels they displayed rusting after exposures of 0.05 dpa and higher. To prevent this rusting, the higher dose specimens were sealed in aluminum envelopes. The envelopes were constructed from very soft, high purity aluminum foil, 0.125 mm thick. Each close-fitting envelope contained one specimen. The envelope was sealed with an electron beam weld in a vacuum chamber. On removal from the chamber, atmospheric pressure forced the soft foil into good contact with the specimen. This contact was reinforced by a light finger squeeze and was maintained by the water pressure during irradiation. It is believed to have ensured that the temperature of the enveloped specimens during irradiation was the same or very close to that for the lower dose bare specimens.

The neutron spectrum at the various stacking positions in the HFIR hydraulic tube is well measured [10] and is reproduced from one fuel cycle to the next. A desired neutron exposure can be achieved simply by controlling the exposure time. Exposure conditions used in the present work are summarized in Table 2. The thermal neutron flux, $E < 0.025$ eV, not given in the table, is larger than the fast flux, $E > 1$ MeV, by a factor of approximately 5.3. Nominal displacements per atom (dpa) levels range from 0.00057 to 1.2 dpa and are estimated from the fast neutron fluences using an atomic displacement cross-section of 1542 b calculated for iron in the neutron spectrum for the HFIR flux trap [11].

Table 2
Irradiation doses

Exposure time	Fluence, $E > 1$ MeV ($\times 10^{24}$ n m^{-2})	dpa
15 min	0.0037	0.00057
1.5 h	0.022	0.0034
6.5 h	0.096	0.015
1 day	0.35	0.054
3 days	1.06	0.16
24 days	7.8	1.2

Tensile tests were conducted at room temperature in a static tensile machine at a cross-head speed of 0.008 mm s^{-1}, corresponding to a specimen strain rate of 10^{-3} s^{-1}. Elongations, or engineering strains, were calculated from the recorded cross-head separation using an initial nominal gauge length of 7.62 mm. The specimen gripping scheme utilizes pins and extension rods which reduce the stiffness of the system and introduce artificially large elastic extensions into the recorded test curves. These elastic extensions are allowed to remain in the displayed test curves but are subtracted to obtain the uniform and total plastic elongations. Engineering stresses were calculated as the applied load divided by the initial cross-sectional area.

The tensile properties of the HFIR-irradiated steels were compared with data available for two of the steels, Fe–9Cr–1MoVNb and Fe–9Cr–2WVTa, after spallation irradiations. The spallation irradiations were conducted in the LANSCE facility at Los Alamos National Laboratory where the specimens were exposed to 800 MeV protons and spallation neutrons at temperatures of 60–164 °C, receiving doses of 0.026–10 dpa, as described in more detail in [12,13].

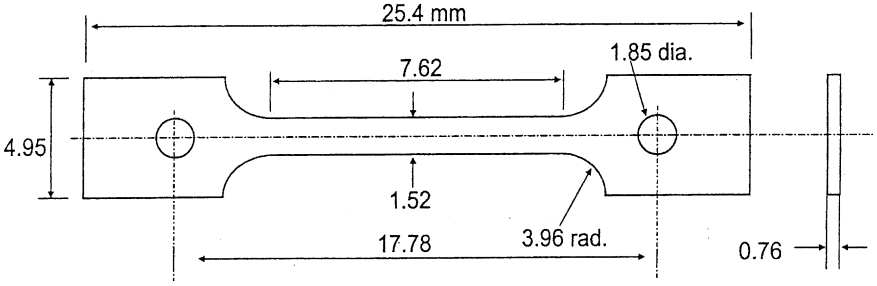

Fig. 1. Dimensions of the SS-3 tensile specimen.

3. Results and discussion

In the unirradiated conditions (Fig. 2(a)) the nickel-doped steel was considerably stronger and less ductile than the others. The three, low-nickel 9Cr steels exhibited intermediate mechanical strengths. The 3Cr–3WV bainitic steel was weaker, and the bainitic A533B steel was the weakest. None of the four F/M steels showed yield perturbations of the type characteristic of ferritic steels; they underwent smooth transitions from elastic to plastic strain. The two bainitic steels had mild discontinuities at yield. All unirradiated steels displayed substantial work hardening, and the associated uniform elongations contributed one third to one half of the total elongation values.

Irradiations in the HFIR caused large increases in strengths and reductions in elongations. Examples of tensile curves for all the steels after two irradiation doses are shown in Fig. 2. The curves for the other four doses showed the same pattern of radiation-induced changes. As shall be shown more clearly in the following sections, the changes for each steel were remarkably similar and consistent at a given dose. Often, irradiation will enhance a preexisting yield point perturbation or will induce one. No yield point perturbations were induced in the four F/M steels. In the two bainitic steels, irradiation caused modest yield point drops. Irradiation reduced the slopes of the work hardening regions of the tensile curves of all the steels and correspondingly shortened their uniform elongations. Indeed, most of the losses in elongations after irradiation were due to curtailment of uniform elongation. The elongations after the UTS, i.e. the necking strains, were relatively less diminished. No measurements were made of reductions-in-area but the long, drawn-out tails on the tensile curves portray considerable necking, indicative of large reductions-in-area. This is quite evident in Fig. 2(c) where the steels all demonstrate prompt necking instability very shortly after yielding yet show substantial total elongation. Almost all of this elongation occurred under the multiaxial loading conditions that prevailed during necking, and it indicates that ductility during multiaxial loading is much less affected by irradiation than is ductility during the conditions of greater uniaxiality that exist before necking. No truly brittle behavior was seen in these tests.

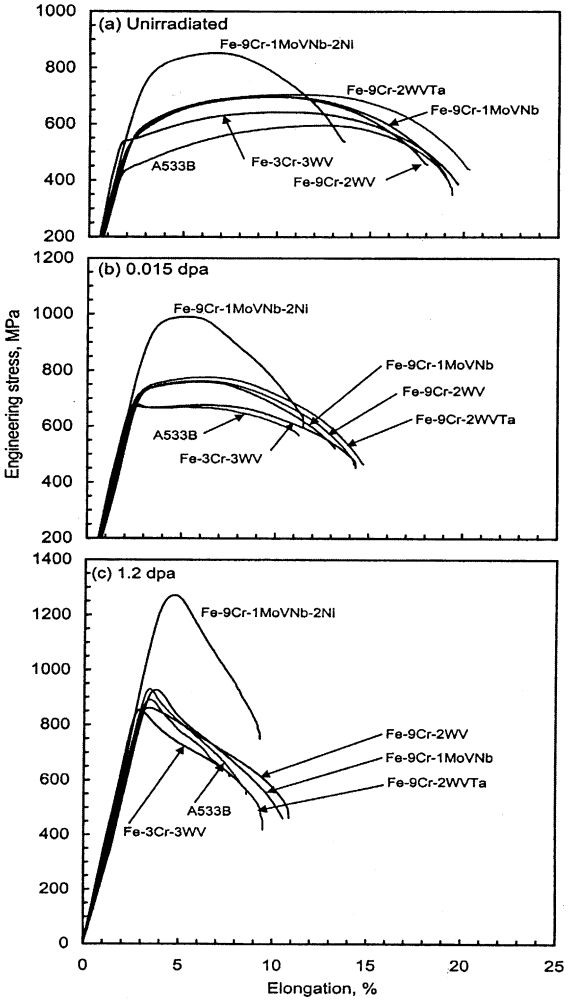

Fig. 2. Examples of the engineering stress–elongation curves for (a) the unirradiated steels, (b) after irradiation to 0.015 dpa, and (c) irradiated to 1.2 dpa.

Although Fig. 2(c) is for a dose of 1.2 dpa, the shapes of the curves, i.e. prompt necking instability at yield and extended necking strain are typical for all doses between 0.05 and 1.2 dpa. At lower doses, yielding was followed by work hardening, albeit less than in the unirradiated controls.

The overall changes in tensile properties with irradiation dose for all the steels are displayed in Fig. 3. Irradiation raised the yield strengths and UTS values (Fig. 3(a)). The Ni-doped steel maintained its strength advantage at all doses. The three low-nickel F/M steels behaved as a close-knit group. The strengths of the originally weaker bainitic steels became similar to the low-nickel F/M steels at doses above about 0.05 dpa. The strengths of the LANSCE irradiated steels were similar to their HFIR-irradiated counterparts at equivalent doses, at least up to 2 dpa. Elongations were reduced by irradiation (Fig. 3(b)). The total elongations decreased gradually with dose whereas the uniform elongations fell rather abruptly to values of 1% or less at doses of 0.05 dpa and higher, coincident with the onset of prompt necking at yield.

3.1. Comparison with hardening models

The dose dependencies of the radiation-induced increases in yield strengths were explored in terms of the popular models based on barrier hardening theory. The

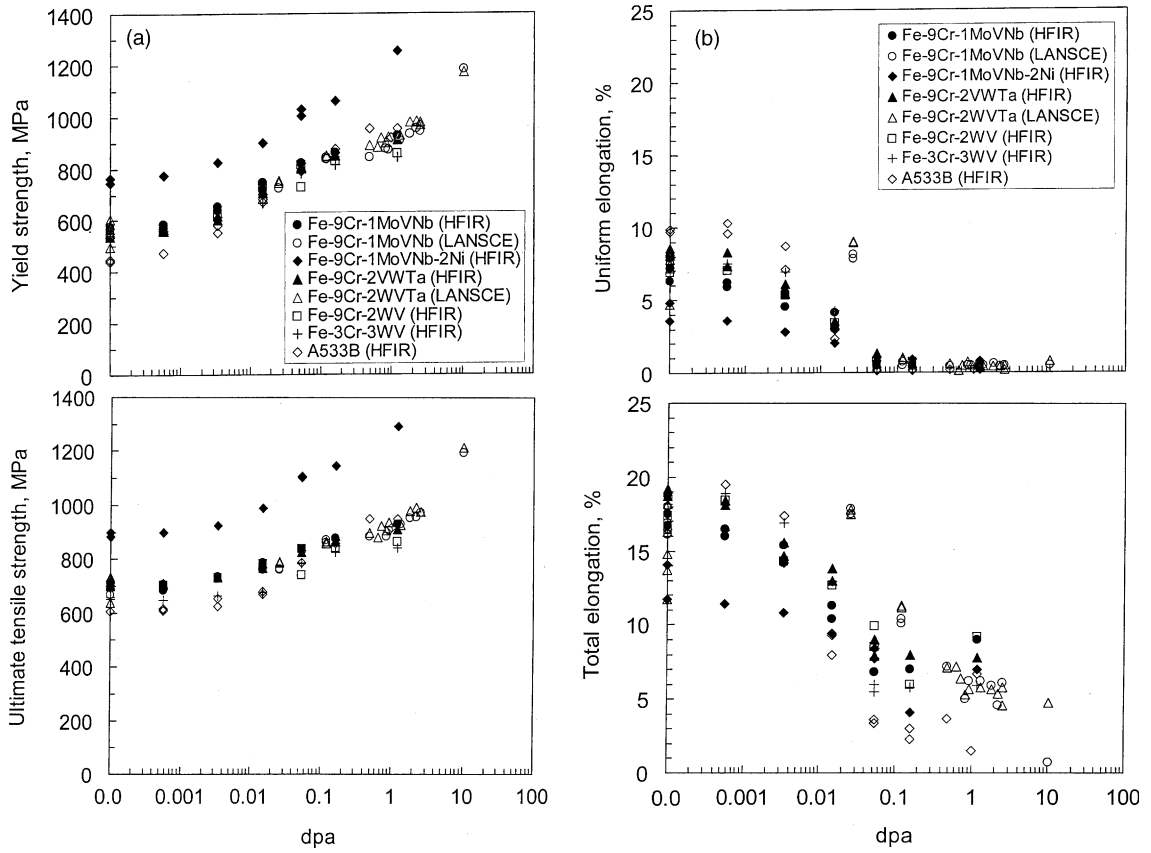

Fig. 3. (a) Fluence dependencies of strength properties; (b) fluence dependencies of tensile elongation values.

earliest models of radiation strengthening [14–16] were in the form of a power law expression $\Delta\sigma_y = h(\Phi t)^n$ in which the barriers are assumed to scale with fluence, Φt, or with dpa. In the low dose regime, the hardening exponent, n, for most metals is claimed to be 1/2 [15,16], but values of 1/3 [14] and 1/4 [17] have been reported for copper. Such scaling should become invalid at higher doses because of cascade overlapping which should diminish the rate of production of new barriers and reduce the value of n. To account for this, a saturation term was introduced [18,19], $\Delta\sigma_y = A(1 - e^{-\Phi t})^{1/2}$. Note that this equation retains an exponent of 1/2, which forces the issue to a preconceived view. A more appropriate expression would be $\Delta\sigma_y = B(1 - e^{-\Phi t})^m$, where the exponent, m, is not preset, but is likely to change with dose or hardening mechanism. For the present purposes, and to avoid the complications of assigning physical meaning to the parameters of the saturation expression, we have taken the simple route of plotting the data for each steel in a log–log format and seeking a pattern. It is found that the plots are remarkable similar to one another. An example for the Fe–9Cr–1MoVNb F/M steel is shown in Fig. 4, and the parameter values for all the steels are listed in Table 3, including those for the LANSCE data.

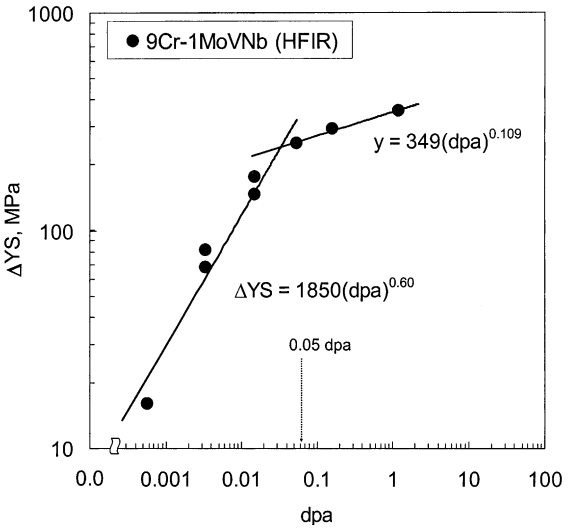

Fig. 4. Example of determination of radiation strengthening coefficients.

It is clear from Fig. 4 that there is a change in slope in the plot at a dose of about 0.05 dpa above which the

Table 3
Coefficients of the dose dependence of the increase in yield stress, $\Delta\sigma_y = h(\mathrm{dpa})^n$

Material	Radiation source	(1) 0–0.05 dpa		(2) >0.05 dpa	
		h_1	n_1	h_2	n_2
Fe–9Cr–1MoVNb	HFIR	1850	0.60	350	0.11
Fe–9Cr–1MoVNb	LANSCE			350	0.18
Fe–9Cr–1MoVNb–2Ni	HFIR	1300	0.53	470	0.21
Fe–9Cr–2VWTa	HFIR	1740	0.60	360	0.11
Fe–9Cr–2VWTa	LANSCE			370	0.17
Fe–9Cr–2WV	HFIR	1230	0.53	320	0.11
Fe–3Cr–3WV	HFIR	1590	0.62	290	0.07
A533B	HFIR	2200	0.56	510	0.11

dose exponent is significantly reduced. From Table 3, the dose exponents below 0.05 dpa are 0.5–0.6 for the HFIR irradiations; above 0.05 dpa they are 0.07–0.11, with the exception of the 9Cr–1MoVNb–2Ni F/M steel which had an exponent of 0.21. No distinction can be seen between the F/M steels and the bainitic steels. With regard to the LANSCE-irradiated F/M steels, there are no data for doses below about 0.02 dpa; for doses above 0.05 dpa their exponents were 0.17–0.18. Thus, for the most part, the HFIR-irradiated steels have exponents of about 1/2 in the low-dose regime, reducing to about 1/10 at doses beyond 0.05 dpa. The HFIR-irradiated nickel-doped F/M steel and the LANSCE-irradiated F/M steels have exponents of about 1/5 at doses above about 0.05 dpa.

The exponents of 1/2 for the lower dose regime, coupled with the prominent knees at 0.05 dpa (3×10^{23} n m^{-2}, $E > 1$ MeV), agree with values reported for other low-dose ferritic materials, as reviewed in Ref. [20]. Reduction in n at doses above 0.05 dpa could be due to cascade overlap which is claimed to occur in iron at a fast fluence of 2.6×10^{23} n m^{-2} corresponding to about 0.04 dpa [21], or at 0.01 dpa [22]. However, that may not be the full answer. A troublesome aspect is that cascade overlap in a barrier hardening model cannot explain the concurrent reductions in work hardening found herein at doses above about 0.05 dpa. A barrier hardening mechanism should give either increasing rate of work hardening with increasing barriers (increasing dose) if the barriers are Orowan type and the dislocations have to loop around them, or it should give less strain hardening if the barriers are shearable. It should not give prompt plastic instability failures, and the elongation during necking should be much less than the uniform elongation, as it is in the unirradiated control specimens. These property changes are too pronounced and too systematic with dose to be mere coincidences. We deduce, therefore, that a barrier hardening mechanism is inappropriate or it has only limited application. We propose that a change in mode of plastic deformation occurs at doses above 0.05 dpa and it contributes to, or controls, the reduction in hardening at the higher doses.

3.2. Change in deformation mode

Strictly, barrier hardening models from which the hardening parameters are derived, address only the very earliest stages of plastic deformation; they estimate the stress level required to force a dislocation through or around the first rank of an array of obstacles. The models say nothing about the subsequent progress of deformation. It is implicit, however, that the plastic deformation mechanism involved does not change with dose; only the magnitude of the required breakaway stress is changed, commiserate with the changes in barrier strength. In principle, the breakaway stress should equate in the tensile test with a sharply defined elastic limit or with the upper yield stress if a yield point drop is involved. In practice, neither of these properties is easily measurable, so the models are usually applied by default to the stresses associated with lower yield points or plastic offsets, both of which involve some measurable degree of plastic deformation. It follows that the parameters derived from the models using these metrics will not be constants if the deformation mode changes with dose (or stress). The change might be as simple as a Orowan-type barrier becoming shearable at high dose (stress). Our tensile data imply strongly that the deformation mode changes at the knees in the log–log plots.

In the irradiated specimens, the loss of work hardening and increasing propensity for early onset of plastic instability failure, coupled with high necking strains, indicate pronounced changes in the mode of deformation that are in agreement with the characteristics of the phenomenon of dislocation channel deformation [23,24], which involves work softening and highly localized deformation. During dislocation channeling, plastic deformation is confined to narrow bands, or channels, on slip systems containing the highest resolved shear stresses. In the channels the radiation damage microstructure is destroyed by glissile dislocations. Since there is no commingling of dislocations in the channels, there is little or no work hardening except at the intersections of channels with one another and with grain boundaries. Very large strains occur in the channels compared to the

relatively undeformed matrix, but the overall bulk elongation and the bulk work hardening rate are reduced. We surmise that relatively high strains in the necked region will result from activation of new channels on previously dormant slip systems by the change from uniaxial to multiaxial stress state when the neck is initiated. No search for dislocation channels by TEM was made in the present work, but there is no question they can occur in irradiated iron and ferritic steels under the irradiation and test conditions used here. They have been reported in neutron irradiated α-iron after doses of about 0.4 dpa at about 50 °C [25,26]; in annealed, untempered Fe–12Cr alloy after irradiation with 590 MeV protons at room temperature to a dose of 0.2 dpa [27]; in F82H F/M steel after neutron irradiation at 300 °C to 5 dpa [28]; and in tempered bainintic A533B steel after neutron irradiation at 65–100 °C to 0.9 dpa [29], all after tensile tests at ambient temperatures. It is important to note that channels can be seen in TEM only when there is visible radiation damage microstructure to provide a contrasting background that highlights the cleared channels. In iron and ferritic steels, the clusters responsible for radiation hardening are very small and are not discernable in TEM until the dose exceeds about 10^{23} n m^{-2} (~0.01 dpa) [30,31] even though hardening can be detected at doses as low as $\sim 1.2 \times 10^{19}$ n m^{-2} (~0.000002 dpa) in pure iron [32] and 1.4×10^{20} n m^{-2} (0.00002 dpa) in alloys [33]. Other techniques such as positron annihilation spectroscopy and electrical resistivity can detect the submicroscopic damage clusters [34]. In the present work, radiation hardening begins at a dose of about 0.0005 dpa, and symptoms of work softening are seen at a dose of 0.05 dpa. At 0.05 dpa, radiation damage microstructure would be present but would probably be hidden by the residual high dislocation densities in the tempered martensite microstructure, and any dislocation channels introduced during straining would not be recognizable.

3.3. Trend curve

The close similarity of the $\log \Delta\sigma_y$ versus log dpa plots for each steel suggest that the plot basis may be useful for constructing the framework for an irradiation hardening trend curve for F/M materials. By considering the radiation-induced increases in yield strengths, instead of the absolute values of yield strengths, any differences due to heat treatment are eliminated. Fig. 5 is such a trend curve for irradiations and tests made at temperatures of 50–160 °C. The curve is offered for collation purposes, not for critical analyses. All published data for F/M steels irradiated at temperatures below about 160 °C are included [2–7,35,36] and they extend the dose range to 24 dpa. Except for the OPTIMAX A steel irradiated with 590 MeV protons in the PIREX facility [6] all the data conform to the trend.

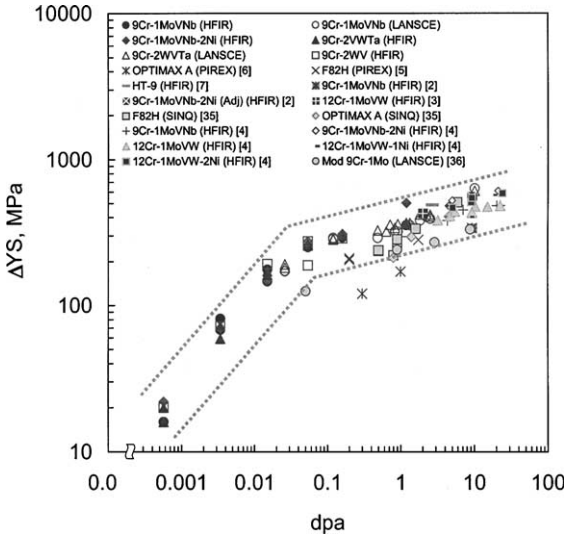

Fig. 5. Trend curve for increases in yield strengths of F/M steels irradiated at temperatures of 50–160 °C.

Even the 9Cr–1MoVNb–2Ni steel is consistent. Previous data for this steel, mostly at higher irradiation temperatures, has indicated excessive radiation hardening attributed controversially to either a difference in heat treatment or to radiation-induced generation of helium [2,37,38] or to precipitation [39,40]. In the present work for irradiations below 100 °C, the addition of 2% nickel to 9Cr–1MoVNb steel alters the unirradiated tensile properties of the steel and causes a small increase in irradiation hardening at doses >0.05 dpa. In the n_2 column of Table 3, this steel has an exponent of 0.21, versus 0.17–0.18 for the two LANSCE-irradiated steels and 0.11 for most of the other conditions. It is tempting to unilaterally attribute the higher exponents to their higher helium contents, but it is not that simple. Estimated helium concentrations are 0.3 appm for the non-nickel steels irradiated to 1.2 dpa in HFIR, and about 8 appm for the 2% nickel steel, whereas the two LANSCE-irradiated steels are expected to contain about 120 appm at 1.2 dpa. So, there is not a systematic relationship between exponent and helium content. A confounding factor may be the higher irradiation temperatures experienced by the LANSCE steels. In Fig. 5, the data labeled LANSCE; SINQ; PIREX; and –Ni HFIR in the legend all have high He/dpa ratios. Those data span the dose range 0.01–24 dpa, with helium contents expected to reach about 1000 appm for the spallation irradiations. A line drawn through this group has a slope of 0.16. Within this group, the steepest slope of 0.33 is exhibited by the OPTIMAX A steel irradiated in PIREX [35]. However, in spite of these signs that might be interpreted as an effect of helium, the evidence is not unambiguous. It is concluded that the present data offers hints, but not incontrovertible evidence, of an effect of

helium on the tensile properties of F/M steels irradiated at temperatures <160 °C.

4. Summary and conclusions

Tensile properties of four ferritic/martensitic steels, 9Cr–1MoVNb, 9Cr–1MoVNb–2Ni, 9Cr–2WV, 9Cr–2WVTa, and a 3Cr–3WV bainitic steel, and a reference pressure vessel steel, A533B, were investigated after irradiation in the HFIR to doses up to 1.2 dpa at temperatures in the range 60–100 °C. Tensile tests were performed at room temperature at a strain rate of 10^{-3} s^{-1}. The following conclusions were drawn:

- These data fill a large gap in the information base for radiation effects on properties of F/M steels for irradiation temperatures <160 °C.
- Considerable radiation strengthening and losses in elongation were found at doses as low as 0.05 dpa.
- Despite large differences in compositions and strengths, the radiation responses of all four F/M steels and the two tempered bainite steels were remarkably similar.
- All the steels irradiated to doses of 0.05 dpa and higher failed by prompt plastic instability, occurring at, or immediately after, the yield point.
- Loss in elongation occurred primarily by reduction of uniform elongation.
- Necking strains were large and were less affected by irradiation than were the uniform elongations.
- All fractures were ductile.
- The presence of nickel in the 9Cr–1MoVNb–2Ni steel increased the unirradiated strength and caused slightly more radiation hardening at doses above 0.05 dpa.
- Radiation strengthening was marginally greater in the 9Cr–1MoVNb and 9Cr–2WVTa steels that were irradiated with 800 MeV protons and spallation neutrons at temperatures of 60–164 °C to doses of 0.026 to 10 dpa in the LANSCE facility at Los Alamos National Laboratory.
- Dose dependencies of the increases in yield strengths for all the steels shared an exponent of 0.5–0.6 for doses below 0.05 dpa (3×10^{23} n m^{-2}, $E > 1$ MeV), and exponents of 0.1–0.2 at higher doses. The critical dose of 0.05 dpa is consistent with claims of saturation of the radiation damage microstructure by cascade overlap, but cascade overlap does not explain the marked reductions in work hardening and elongation found at doses above 0.05 dpa. It is proposed that at doses above 0.05 dpa the yield strength is compromised by intervention of dislocation channeling deformation, which induces prompt plastic instability failure at yield.
- A suggestion is made for a trend curve for correlating changes in yield strength with dose.
- There are signs of a small radiation strengthening contribution attributable to the presence of helium.

Acknowledgements

This research was sponsored by the Spallation Neutron Source Project, Office of Science, US Department of Energy, under contract DE-AC05-00OR22725 with UT-Battelle, LLC. We are indebted to Drs S.A. Maloy and W.F. Sommer of Los Alamos National Laboratory for their cooperation with the LANSCE irradiations.

References

[1] R.L. Klueh, D.R. Harries, High Chromium Ferritic and Martensitic Steels for Nuclear Applications, ASTM MONO3, American Society for Testing and Materials, 2001.
[2] R.L. Klueh, J.M. Vitek, M.L. Grossbeck, Eleventh Conference, ASTM STP 782, American Society for Testing and Materials, 1982, p. 648.
[3] R.L. Klueh, J.M. Vitek, Ferritic Materials for Use in Nuclear Energy Technologies, Metal. Soc. AIME, 1984, p. 615.
[4] R.L. Klueh, J.M. Vitek, J. Nucl. Mater. 161 (1989) 13.
[5] P. Spatig, R. Schäublin, S. Gyger, M. Victoria, J. Nucl. Mater. 258–263 (1998) 1349.
[6] N. Baluc, C. Bailat, Y. Dai, M.I. Luppo, R. Schäublin, M. Victoria, Mater. Res. Soc. Proc. 54 (1999) 539.
[7] A.F. Rowcliffe, J.P. Robertson, R.L. Klueh, K. Shiba, D. Alexander, M.L. Grossbeck, S. Jitsukawa, J. Nucl. Mater. 258–263 (1998) 1275.
[8] R.L. Klueh, J.M. Vitek, W.R. Corwin, D.J. Alexander, J. Nucl. Mater. 155–157 (1988) 973.
[9] R.L. Klueh, D.J. Alexander, P.J. Maziasz, Met. Mater. Trans. 28A (1997) 335.
[10] S.T. Mahmood, S. Mirzadeh, J.V. Pace III, K. Farrell, B.M. Oliver, ORNL/TM-12831, Oak Ridge National Laboratory Report, December 1994.
[11] T.A. Gabriel, B.L. Bishop, F.W. Wiffen, ORNL/TM-6361, Oak Ridge National Laboratory Report, August 1979.
[12] K. Farrell, T.S. Byun, SNS/TR-211, Oak Ridge National Laboratory Report, January 2001.
[13] K. Farrell, T.S. Byun, J. Nucl. Mater. 296 (2001) 129.
[14] T.H. Blewitt, R.R. Coltman, R.E. Jamison, J.K. Redman, J. Nucl. Mater. 2 (1960) 277.
[15] D.K. Holmes, Solid State Division Annual Progress Report, ORNL-2413, Oak Ridge National Laboratory, Oak Ridge, TN, November 1957, p. 13.
[16] A.K. Seeger, Proceedings of the 2nd International Conference On Peaceful Uses of Atomic Energy, vol. 6, 1958, p. 250.
[17] S.J. Zinkle, J. Nucl. Mater. 150 (1987) 140.
[18] A.D. Whapham, M.J. Makin, Philos. Mag. 5 (1960) 237.
[19] M.J. Makin, F.J. Minter, Acta Met. 8 (1960) 691.
[20] E.A. Little, Int. Met. Rev. 204 (1976) 25.
[21] J.R. Beeler, Flow and Fracture Behavior of Metals and Alloys in Nuclear Environments, ASTM STP 380, American Society for Testing and Materials, 1964, p. 86.

[22] F. Gao, D.J. Bacon, A.F. Calder, P.E.J. Flewitt, T.A. Lewis, J. Nucl. Mater. 230 (1996) 47.
[23] F.A. Smidt Jr., Dislocation channeling in irradiated metals, NRL Report 7078, Naval Research Laboratory, Washington, DC, 1970.
[24] M.S. Wechsler, The Inhomogeneity of Plastic Deformation, American Society for Metals, 1971, p. 19 (Chapter 2).
[25] B.L. Eyre, A.F. Bartlett, Philos. Mag. 12 (1965) 261.
[26] B.N. Singh, A. Horsewell, P. Toft, J. Nucl. Mater. 271&272 (1999) 97.
[27] M.I. Luppo, C. Bailat, R. Schäublin, M. Victoria, J. Nucl. Mater. 283–287 (2000) 483.
[28] N. Hashimoto, S.J. Zinkle, R.L. Klueh, A.R. Rowcliffe, K. Shiba, Mat. Res. Soc. Symp. Proc. 650 (2001) R1.10.1.
[29] K. Farrell, T.S. Byun, N. Hashimoto, Mapping flow localization processes in deformation of irradiated reactor structural alloys, ORNL/TM-2002/66, Oak Ridge National Laboratory Report, July 2002.
[30] B.L. Eyre, Philos. Mag. 7 (1962) 2107.
[31] I.M. Robertson, M.L. Jenkins, C.A. English, J. Nucl. Mater. 108&109 (1982) 209.
[32] G.P. Seidel, Radiat. Effects 1 (1969) 177.
[33] K. Farrell, S.T. Mahmood, R.E. Stoller, L.K. Mansur, J. Nucl. Mater. 210 (1994) 268.
[34] M. Eldrup, B.N. Singh, S.J. Zinkle, T.S. Byun, K. Farrell, J. Nucl. Mater. 307–311 (2002) 912.
[35] Y. Dai, S.A. Maloy, G.S. Bauer, W.F. Sommer, J. Nucl. Mater. 283–287 (2000) 513.
[36] S.A. Maloy, M.R. James, G. Wilcutt, M. Sokolov, L.L. Snead, M.L. Hamilton, F. Garner, J. Nucl. Mater. 296 (2001) 119.
[37] R.L. Klueh, D.J. Alexander, J. Nucl. Mater. 187 (1992) 60.
[38] R. Kasada, A. Kimura, H. Matsui, M. Narui, J. Nucl. Mater. 258–263 (1998) 1199.
[39] D.S. Gelles, J. Nucl. Mater. 230 (1996) 187.
[40] R.L. Klueh, D.J. Alexander, J. Nucl. Mater. 230 (1996) 191.